Applied Catalysis B: Environmental 181 (2016) 692–698

Contents lists available at ScienceDirect

Applied Catalysis B: Environmental

journal homepage: www.elsevier.com/locate/apcatb

Comparison of MoO_3 and WO_3 on arsenic poisoning V_2O_5/TiO_2 catalyst: DRIFTS and DFT study

Yue Peng[a,b], Wenzhe Si[a], Xiang Li[a], Jinming Luo[b], Junhua Li[a,*], John Crittenden[b,*], Jiming Hao[a]

[a] State Key Joint Laboratory of Environment Simulation and Pollution Control, School of Environment, Tsinghua University, Beijing 100084, China
[b] School of Civil and Environmental Engineering and the Brook Byers Institute for Sustainable Systems, Georgia Institute of Technology, Atlanta, Georgia 30332-0595, United States

ARTICLE INFO

Article history:
Received 17 May 2015
Received in revised form 12 August 2015
Accepted 14 August 2015
Available online 20 August 2015

Keywords:
SCR catalyst
Arsenic resistance
MoO_3
DRIFTS
DFT

ABSTRACT

The mechanisms of arsenic poisoning on MoO_3- and WO_3-doped V_2O_5/TiO_2 catalysts are studied and the poisoning resistance effect of MoO_3 are revealed. The arsenic at certain amount (above 10% of arsenic from XPS) decreases the surface area and the number of active sites where reduction takes place. From the results of DRIFTS and DFT, arsenic lowers the surface acidity by decreasing the quantity of Lewis acid sites and the stability of Brønsted acid sites. We also found newly formed As–OH groups of poisoned catalysts (at 1440 cm^{-1}) have quite low activity at high temperature.

MoO_3 provides better activity on poisoned catalysts than WO_3 does on V_2O_5/TiO_2 catalysts. This may be due to the good dispersion of MoO_3 on the support. The reactivity of surface W–O–W and W = O groups is considerably lower than the corresponding Mo–O–Mo and Mo = O groups from the DFT calculations models. This could be one of the explanations on the decrease of surface acidity of poisoned catalysts.

1. Introduction

NO_x emitted from coal-fired power plants and industrial boilers is the main air pollutants, which produce particulate matter and has a serious environmental and human health impacts. Accordingly, the abatement of NO_x is one of the key steps for improving air quality. Selective catalytic reduction (SCR) of NO_x with NH_3 is an effective method. NH_3 (or urea solutions) is used in the presence of excess O_2, and reacts with NO_x to form H_2O and N_2 [1,2]. Commercial SCR catalysts are V_2O_5–WO_3(MoO_3)/TiO_2, where V_2O_5 is active sites with uniform monolayer dispersion. The addition of WO_3 or MoO_3 increases the catalytic activity and thermal durability by stabilizing TiO_2 preventing a phase change from anatase to rutile. The TiO_2 anatase provides good resistance to SO_2 fouling and sufficiently large surface area for high dispersion of V_2O_5 [3,4]. Nevertheless, there are still several problems on catalysts, for example toxicity of V_2O_5 to human, high conversions of SO_2 to SO_3 and deactivation by alkali metals or arsenic in the flue gas. These poisons not only decrease SCR performance, shorten catalysts working lifetime, but also plug the module or monolith pores of catalytic convertor, even corrode the pipeline and increase the backpressure [5–9].

Arsenic (As) is a serious poison for SCR catalysts, and can be found as As_2O_3 with concentrations from 1 $\mu g/m^3$ to 10 mg/m^3 [10]. Previous studies reported that arsenic had a valence of +5 and was bonded to both V_2O_5 and TiO_2 [11]. Our recent works on potassium [12–14] and arsenic [15,16] poisoning show that K_2O decreases both Brønsted acid sites and reducibility of catalysts by tightly bonding to active sites, whereas arsenic decreases Lewis acid sites and slightly improves reducibility by forming unstable arsenic hydroxyls (As–OH). In addition, nearly half of arsenic could be effectively removed by 4% H_2O_2 solution, which could be a possible method of catalysts regeneration [15].

Compared with WO_3, MoO_3 has a promotion effect on arsenic poisoned V_2O_5/TiO_2, but the specific mechanism of this inhibition is still unclear [17,18]. Some researchers propose that the structural and morphological characteristics of MoO_3 and WO_3 on TiO_2 are similar [19], yet, two questions still need to be answered: First, why do we find more N_2O formed on MoO_3/TiO_2 than WO_3/TiO_2? Secondly, whether the surface species of poisoned catalysts are the same or similar as fresh catalysts [20]? Therefore, in order to design arsenic poisoning resistance catalysts, it is necessary to elucidate the different poisoning behaviors of WO_3 and MoO_3 on V_2O_5/TiO_2. Moreover, from theoretical point view, many published works have

* Corresponding authors. Fax: +1 404 894 5676.
E-mail addresses: lijunhua@tsinghua.edu.cn (J. Li), john.crittenden@ce.gatech.edu (J. Crittenden).

http://dx.doi.org/10.1016/j.apcatb.2015.08.030
0926-3373/

successfully constructed the V_2O_5 cluster or slab models supported on low index planes of TiO_2 [21–23]. Some studies have investigated poisoning mechanisms of alkali metals and lead on active sites [24,25]. However, few works have been focused on arsenic [26].

In this work, V_2O_5–MoO_3/TiO_2 and V_2O_5–WO_3/TiO_2 catalysts are prepared to investigate the poisoning mechanism of arsenic by DRIFTS and density functional theory (DFT) methods. We try to clarify the relationship between surface species and catalytic activity, and the universal DFT models for SCR are also provided.

2. Experiment and calculation

2.1. Catalyst preparation and poisoning

The catalysts are prepared by wet impregnation methods. The content of V_2O_5 is 1 wt.%. MoO_3 loadings are 3 and 1.9 wt.% and WO_3 loading is 3 wt.%, which is the same molar ratio as that with 1.9 wt.% of MoO_3. TiO_2 anatase is used as support. Samples are first dried and calcined at 500 °C for 5 h, and then sieved within 40–60 meshes for activity measurement and with more than 60 meshes for physi–chemical characterizations. They are denoted as fresh samples: F3%Mo, F3%W and F1.9%Mo. The corresponding poisoned samples are obtained by introducing As_2O_3 stream (As_2O_3 is placed in the tube furnace at 350 °C before the catalyst. Stream (3% H_2O/N_2) is introduced into the rube furnace, carrying the vaporized As_2O_3 to the catalyst.) The catalyst (40–60 meshes) then is exposed to an O_2-rich stream (3% O_2/N_2) for 72 h at 370 °C. They are denoted as poisoned samples: P3%Mo, P3%W and P1.9%Mo. The catalysts P3%W and P1.9%Mo are also washed by 4% H_2O_2 solution to remove part of arsenic. They are denoted as R3%W and R1.9%Mo.

2.2. Catalytic activity

The activity tests are performed in a fixed-bed quartz reactor. The feed gas contains 500 ppm NO, 500 ppm NH_3, 3% O_2 and the balance is N_2 (high purity). The concentrations of outlet gases are monitored using an FTIR spectrometer (GASMET DX- 4000). The results are recorded when the reaction reaches a steady state. To better evaluate the catalytic activity, kinetic parameters are calculated according to the following equation:

$$k = -\frac{v}{w} \times \mathrm{In}(1-x) \quad (1),$$

where k is the reaction rate constant (mL g^{-1} s^{-1}), V is the total flue gas rate, W is the mass of catalyst in the reactor, and x is the NO_x conversion in the testing activity. The equation is based on the understanding that the reaction is pseudo-first order dependent on NO and zero order dependent on NH_3 [4].

2.3. Catalyst characterization

X-ray photoelectron spectroscopy (XPS) is performed with an ESCALab220i-XL electron spectrometer from VG Scientific using 300 W AlKα radiations. The binding energy is referenced to the C1s line at 284.8 eV. The elements contents are characterized by ICP-AES with an IRIS Intrepid II XSP apparatus (Thermo Fisher Scientific Inc.). BET surface area is carried out with a Micromeritics ASAP 2020 apparatus. Temperature programmed reduction (TPR) of H_2 is performed on a chemisorption analyzer (Micromeritics, ChemiSorb 2920 TPx) under 10% H_2/Ar flue gas (50 mL/min) at a rate of 10 °C/min up to 800 °C. DRIFTS spectra are recorded on an online Fourier transform infrared spectrometer (FTIR, Nicolet NEXUS 870) equipped with the Harrick IR cell and an MCT detector cooled by liquid N_2. Each sample is first pretreated in N_2 (200 mL/min) gas at 350 °C for 1 h. The background spectrum is collected in a N_2 atmosphere and subtracted from the sample spectra. The IR spectra are recorded by accumulating 64 scans and the resolution is 4 cm^{-1}. To diminish the influence of absorbance for different samples, the absorbance intensity is set to 2.50 for each sample at 100 °C.

2.4. Model selection and calculation detail

Although the (1 0 1) surface is more stable and commonly investigated than (0 0 1), the (0 0 1) and (1 0 0) faces are found in the industrial TiO_2 powders and show higher catalytic activity [27] . The TiO_2 anatase (001) surface is reconstructed by a (3 × 3) supercell of the slab model. A vacuum gap of 15 Å is used to separate subsequent slabs ($(TiO_2)_{36}$). Based on recent works on TiO_2 (0 0 1) [28,29], a 3-layer slab is sufficient because of its self-driven reconstruction when it is cleaned under vacuum conditions [21]. For the surface relaxation, the bottom layer is fixed to the bulk parameter, no symmetry is used and a dipole correction is included (Fig. S1 in the Supporting information).

All structural optimizations are based on DFT and performed using the Material Studio 5.5 software with plane-wave basis sets [30]. A plane-wave energy cutoff of 400 eV is used in all cases. The generalized gradient approximation plus Hubbard model (GGA + U) according to Perdew, Burke and Ernzerhof (PBE) is used [31,32], where the value of U is set to 3.5 for Ti [33]. The Monkhorst–Pack division scheme is selected to generate a set of k-point within the Brillouin zone. The adsorption energy (E_{ad}) of NH_3 molecule is calculated as follows:

$$E_{ad} = E_{surf} + E_{NH_3} - E_{tot} \quad (2),$$

E_{surf} is the energy of surface, E_{NH_3} is the energy of an isolated NH_3 molecule and E_{tot} is the total energy of the same molecule adsorbed on surface. Note that a positive value for E_{ad} suggests a stable adsorption.

3. Results and discussion

3.1. SCR performance

Fig. 1 shows the NO_x conversion and N_2O formation of fresh and poisoned catalysts for a GHSV of 120,000 mL/g h. Fresh catalysts reach 100% NO_x conversion above 350 °C, and the activity order at relatively low temperatures (250 °C) is: F3%Mo > F1.9%Mo > F3%W. Poisoned catalysts exhibit lower activities than the corresponding fresh catalysts, nevertheless, their activity order is not changed: 60% and 55% NO_x conversion is obtained for P3%Mo and P1.9%Mo at 450 °C, respectively, while it is only 40% for P3%W. That is, MoO_3 improves SCR activity more than WO_3 on V_2O_5/TiO_2 either in terms of the equal mass or molar ratio of MoO_3 to WO_3. The N_2O concentrations of the catalysts are also measured. Compared to fresh catalysts, poisoned samples produce considerable amount of N_2O at high temperatures, and MoO_3 produces more N_2O than WO_3. Previous study also showed the similar results, and N_2O has about 300 times more global warming potential than CO_2, the increased N_2O comes from the unselective oxidation on As_2O_5 [16].

However, the SCR catalysts always work in the presence of H_2O and SO_2. We study NO_x conversion of F3%Mo and P3%Mo catalysts in the presence of 5% H_2O and 200 ppm SO_2 under higher GHSV (Fig. 2). Although NO_x conversion of catalysts inevitably drops when H_2O or SO_2 is introduced below 400 °C, N_2O concentrations are significantly lower after introducing 5% H_2O and further decrease with increased GHSV. In fact the N_2O for F3%Mo is less than 10 ppm at 450 °C as compared to a N_2O of 135 ppm for P3%Mo without H_2O. The inhibition on N_2O formation could be attributed to the competition adsorption of H_2O and NH_3 as well as the decrease of oxidation ability of catalytic surfaces in the presence of H_2O [34]. There is usually 5–10% H_2O in the flue gas of stationary sources, hence the

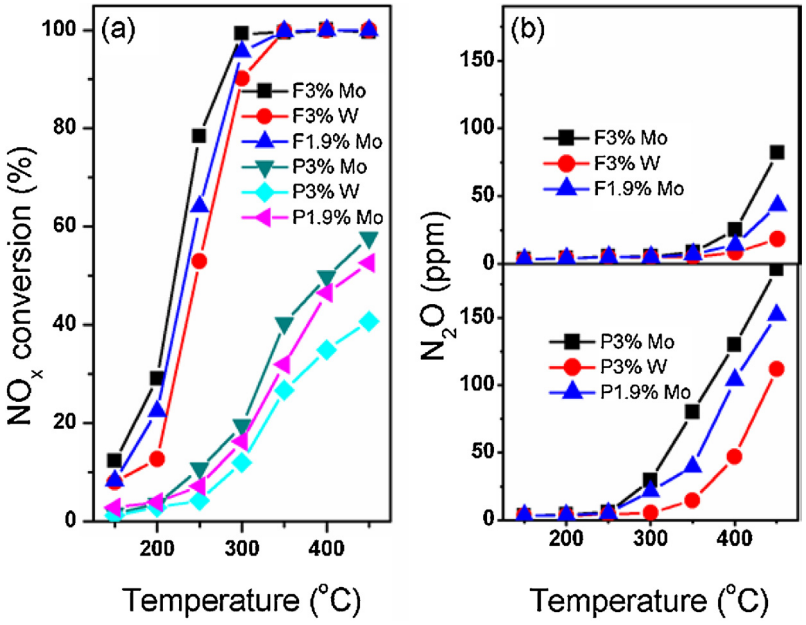

Fig. 1. SCR performance of fresh and poisoned catalysts in the temperature range of 150–450 °C. Reaction conditions: samples mass = 100 mg, [NO] = [NH_3] = 500 ppm, [O_2] = 3%, total flue rate = 200 mL/min, GHSV = 120,000 mL g^{-1} h^{-1}.

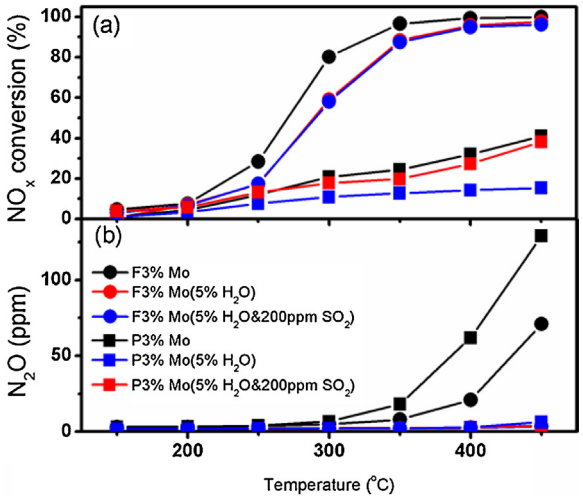

Fig. 2. The influence to SCR performance of high GHSV, 5% H_2O, and both 5% H_2O and 200 ppm SO_2 in the flue gas on F3%Mo and P3%Mo catalysts. Reaction conditions for: samples mass = 50 mg, [NO] = [NH_3] = 500 ppm, [O_2] = 3 %, total flue rate = 200 mL/min, GHSV = 240,000 mL g^{-1} h^{-1}.

influence of MoO_3 on N_2O generation might be neglected under real conditions.

Table 1 summaries the pseudo-first order rate constants based on surface area and mass constants at 200 °C for F3%W and F1.9%Mo. Poisoned and regenerated rate constants are also provided, where the molar ratio of WO_3 and MoO_3 in the two catalysts is the same. The reaction rate of F1.9%Mo is greater than that of F3%W. After arsenic poisoning, the reaction rate constant on the basis of surface area is nearly 60 % lower for F3%W (0.049 mL/m^2 s to 0.020 mL/m^2 s), and the decrease is 50 % for F1.9%Mo (0.088 mL/m^2 s to 0.045 mL/m^2 s). These results confirm that MoO_3 is more resistant to arsenic poisoning than WO_3. As shown in Table 1, the reaction rate constant for R3%W and R1.9%Mo are only slightly greater than those of poisoned catalysts. This could be due to the combined effects of (1) the loss of As (which increases activity), (2) the loss of V (which decreases activity) and (3) considerable decrease of Mo (0.80 % to 0.35 %, which decreases activity).

3.2. Materials texture

Table 1 gives the surface areas and element components. Our previous work shows that the surface area of arsenic poisoned catalyst at low loading (1.40 wt.% As) is small and not an important deactivation factor [16]. However, poisoning decreases the surface area of samples at a certain arsenic amount in this work. Therefore, we believe that large amount of arsenic may decrease the surface area of poisoned catalysts. This point is mute because the amount of poisoning that would occur would render the catalyst useless. XPS (Fig. S2) and ICP were conducted to determine the changes of surface and bulk V, W/Mo and As. Nearly 2/3 of surface V is lost for poisoned catalysts and the surface loading of arsenic are between 11 and 13%. Surface Mo loading increase after As poisoning for F3%Mo and F1.9%Mo and surface W loading decreases slightly for F3%W. The results imply that besides the loss of V active sites, arsenic reduces the surface W loading for WO_3-containing catalysts and increases the surface Mo loading for MoO_3 catalysts. Previous studies on the arsenic poisoning on V_2O_5–MoO_3/TiO_2 proposed that the $As_4Mo_3O_{14}$ phase was formed and identified and it would also transform to a more stable phase ($MoAs_2O_7$) [35]. Under this phase transformation, As^{3+} is oxidized to As^{5+} and Mo^{6+} is reduced to Mo^{4+}, i.e., arsenic could react with neighbored MoO_3 species on the catalyst surface, increasing the cations radii of Mo (Mo^{6+}: 5.5-6.4 Å; Mo^{4+}: 7.9 Å). This could be one of the reasons accounting for the increased amount of Mo from XPS results; however, we didn't found the similar results between WO_3 and arsenic. We propose that As_2O_3 would cover surface WO_3 and V_2O_5 (both the loading of WO_3 and V_2O_5 decreased for poisoned samples from XPS results.)

3.3. Temperature programmed study

Fig. 3(a) displays H_2–TPR profiles of F3%W and F1.9%Mo and poisoned and regenerated samples. Fresh catalysts exhibit two peaks in the temperature range of 400- 600 °C: (1) a peak at 450 °C and a shoulder at 480 °C for F1.9%Mo and (2) a possible overlapped band

Table 1
Surface areas and reaction rates, surface and bulk elements ratios, of fresh, poisoned and regenerated catalysts (M = Mo or W).

	F3%Mo	F3%W	F1.9%Mo	P3%Mo	P3%W	P1.9%Mo	R3%W	R1.9%Mo
SA (m^2/g)	86.3	77.8	88.1	54.2	41.0	50.8	75.2	69.9
k (mL/g s)[a]	8.35	3.81	7.73	3.37	0.82	2.31	4.59	5.59
k' (mL/m^2 s)	0.097	0.049	0.088	0.062	0.020	0.045	0.031	0.050
V (%)[b]	0.42	0.48	0.45	0.12	0.13	0.15	–[d]	–
M (%)[b]	1.74	2.80	1.24	2.40	2.14	2.11	–	–
As (%)[b]	–	–	–	11.61	12.56	11.73	–	–
V (%)[c]	0.59	0.57	0.58	0.42	0.35	0.37	0.13	0.13
M (%)[c]	1.50	0.97	0.88	1.36	0.86	0.80	0.64	0.35
As (%)[c]	–	–	–	3.13	2.92	2.73	1.34	1.73

[a] NO_x conversion at 200 °C.
[b] Calculated by XPS.
[c] Calculated by ICP.
[d] Did not detected or calculated.

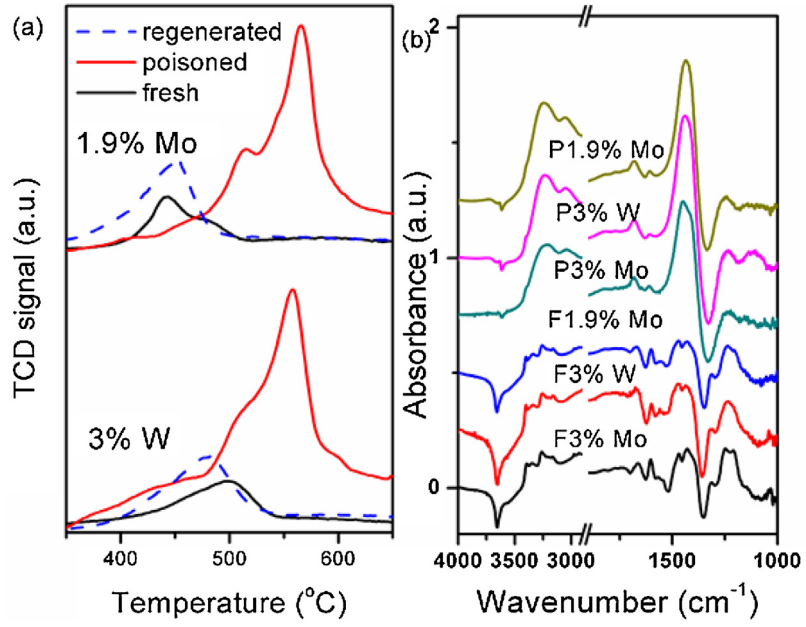

Fig. 3. (a) H_2-TPR profiles in the temperature range of 350-650 °C and (b) DRIFTS spectra of NH_3 adsorptions at 100 °C of catalysts.

centered at 500 °C for F3%W. The low temperature reduction is attributed to the V^{5+} species and the high temperature reduction is attributed to the Mo^{6+} or W^{6+} species [36–38]. The maximum peak of F1.9%Mo (450 °C) is lower than that of F3%W (500 °C), indicating F1.9%Mo has better reducibility than F3%W. As known, N_2O formation is originated from the unselective reduction of NO with NH_3 and the oxidation of NH_3 at high temperatures. They both show directly correlations with reducibility of materials. This could be one of the reasons that F1.9%Mo produces more N_2O above 350 °C than F3%W. Reduction peaks of poisoned catalysts grow up significantly and shift to higher temperature at c.a. 550 °C. Based on the previous studies, the enhanced peaks were assigned to the reduction of both surface V_2O_5 and some new species formed between active sites and As_2O_5 [15,16]. However, we cannot identify the specific species merely based on H_2-TPR. With respect to regenerated samples, nearly half of the arsenic is removed by H_2O_2 solutions, and TPR profiles change significantly. The shapes show similar as their fresh counterparts, but the peaks locations display somewhat movement to higher temperature, i.e., the reducibility of regenerated catalysts is still lower than fresh.

Fig. 3(b) displays the DRIFTS spectra of NH_3 adsorption on fresh and poisoned catalysts at 100 °C. A band within 1150–1300 cm^{-1}, peaks at 1598, 3170 and 3349 cm^{-1} can be attributed to the Lewis acid sites. While a band within 1350–1500 cm^{-1}, peaks at 1685, 3250 and 3385 cm^{-1} can be attributed to the Brønsted acid sites [39]. For fresh catalysts, another peak at 3652 cm^{-1} is also observed. This peak can be attributed to the vibration of —OH [39,40]. When the catalysts are poisoned by As, the vibration of —OH becomes invisible, new peaks at 3225 and 3058 cm^{-1} appear. Furthermore, the band at 1420 cm^{-1} significantly increases, while the changes of the peak at 1685 cm^{-1} is not apparent. Therefore, we cannot simply assign the great band (1420 cm^{-1}) of poisoned samples to Brønsted acid sites. Considering the growth of 1420, 3058 and 3225 cm^{-1} simultaneously, the increase of this band is partially due to the NH_3 adsorption on arsenic oxides: 3058 cm^{-1} might be due to the NH_3 adsorbed on As^{5+}, and 3225 cm^{-1} might be due to the NH_3 adsorbed on As–OH. Here, it must be noted that this assignment is only the speculations. To the best of our knowledge, the assignment of the two peaks has not been reported yet. However, the following DRIFTS and DFT works will give more details about this assignment.

To further study the changes of surface acidity after poisoning and the new peak assignment, DRIFTS spectra under NH_3 desorption and reaction with NO_x are carried out. Considering the inaccuracy amount of Brønsted acidity at 1420 cm^{-1}, two peaks near 1650 cm^{-1} are selected for the semi-quantity of Lewis and Brønsted acid sites with increased temperatures (Fig. 4(a)). Compared with fresh catalysts, Lewis acid sites of poisoned catalysts significantly decrease at 100 °C. With elevated temperatures, they almost disappear up to 300 °C. For Brønsted acid sites, though the amount shows less influenced by poison, the thermal stability sig-

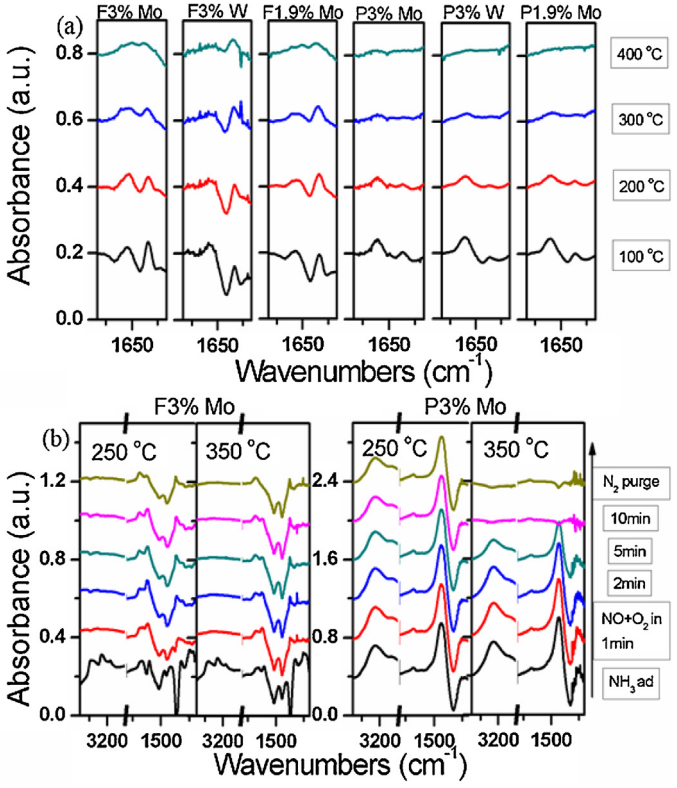

Fig. 4. DRIFTS spectra of (a) NH_3 desorption on fresh and poisoned catalysts from 100 to 400 °C and (b) F3%Mo and P3%Mo catalysts pretreated by 500 ppm NH_3, and then followed by exposing to 500 ppm NO and 3% O_2 at 250 and 350 °C.

nificantly decreases. Part of Brønsted acid sites are observed at 400 °C for fresh catalysts, while only a slight band is obtained from poisoned catalysts. NH_3–TPD profiles are also carried out (Fig. S3), most of the acidity loses at relatively high temperature, which could be due to the less stability of Brønsted acid sites. In order to study the reactivity of adsorbed NH_3 species after poisoning at different temperatures, transient DRIFTS spectra are performed on both F3%Mo and P3%Mo catalysts (Fig. 4(b)). Both Lewis and Brønsted acid sites present active on F3%Mo at 250 and 350 °C, they are totally consumed (3000–3600 cm^{-1}) when NO and O_2 are introduced within 1 min. After that, some surface nitrite or nitrate species are detected (1500–1700 cm^{-1}) [41–43]. Regarding to the spectra of P3%Mo, peaks within 3000–3600 cm^{-1} are nearly unchanged after 10 min at 250 °C and are still considerably after purged by pure N_2 for 30 min. The results imply that NH_3 molecules adsorbed on As are inactive for SCR reaction at 250 °C, which could be one of important evidences of As poisoning. When the temperature is higher to 350 °C, these inactive species begin to reduce at c.a. 2 min and totally disappear at 10 min, indicating that these species only reactive at high temperature. However, the reaction rates are still quite lower than Lewis or Brønsted acid sites (consumed within 2 min). Therefore, we propose that the peaks at 3058 and 3225 cm^{-1} are the vibrations of NH_3 molecules bonding to surface arsenic sites and these adsorbed NH_3 molecules have quite low activity with NO_x.

3.4. DFT study

The specific NH_3 adsorption configurations on V_2O_5/TiO_2 (001) models and the influences of W or Mo and As on them are investigated by DFT calculations. The selected models of the TiO_2 and V_2O_5/TiO_2 have been systemically confirmed and used for the SCR reaction and Hg^0 oxidation [28,29]. Fig. S4 presents the optimized models of VTi, AsTi and AsVTi slabs and the projected density of state (PDOS) of the selected surface atoms. The O 2p states of V = O for VTi decrease compared to those of AsVTi, and the valence band (VB) shifts slightly to the lower energy (−0.38 to −0.57 eV). The results indicate that the reactivity of surface V = O decrease by the influence of As_2O_5 cluster. Fig. 5 shows the NH_3 adsorptions at both Lewis and Brønsted acid sites on VTi, AsTi and AsVTi models. Since the active sites of V_2O_5/TiO_2 catalyst are the surface V = O groups, we only calculate the optimized configurations and the adsorption energies, E_{ad} (labeled on the figure) on these positions. The E_{ad} values of Lewis acidity (**a**, **c**, **e**) are slightly smaller than those of Brønsted acidity (**b**, **d**, **f–h**). This could be accounted for the different binding behaviors: NH_3 bonds to the top sites of the metal cations (V^{5+}, As^{5+}) through an N-down orientation, and these cations accept electrons from the long pair states of N; whereas NH_3 bonds to surface hydroxyl of the H-terminated surface sites. This bondage is usually stronger than Lewis acidity on V_2O_5-based catalysts [44]. Meanwhile both the E_{ad} values on VTi are larger than those of AsTi, especially the Lewis acidity (**a**, **c**), which shows a good accordance with the acid stability discussed in Fig. 4 (a), i.e., As decreases strengthen of both Lewis and Brønsted acid sites. To study the possibilities of NH_3 adsorptions on AsVTi model, we initially put NH_3 molecules near both V = O and As = O group, the bondage near V = O is obtained. The E_{ad} is similar as that of adsorption on VTi (0.85 eV to 0.84 eV). The results indicate that though arsenic prohibits the bonding of NH_3 to As = O, the NH_3 to V = O is just slightly influenced. Further, we also optimize the NH_3 adsorptions on V–OH (**f**) and As–OH (**h**). The results show that NH_3 prefers to form a stable bondage with As–OH. Here we should pay more attentions on the adsorptions of Fig. 5(g), that is the adsorption of NH_3 on As–OH with a neighbored V–OH (competitive Brønsted acid sites adsorption). The original position of NH_3 is in the middle of two –OH sites. After geometry optimization, NH_3 bonds with As–OH rather than V–OH with relatively the highest E_{ad} (1.44 eV) among the DFT cal-

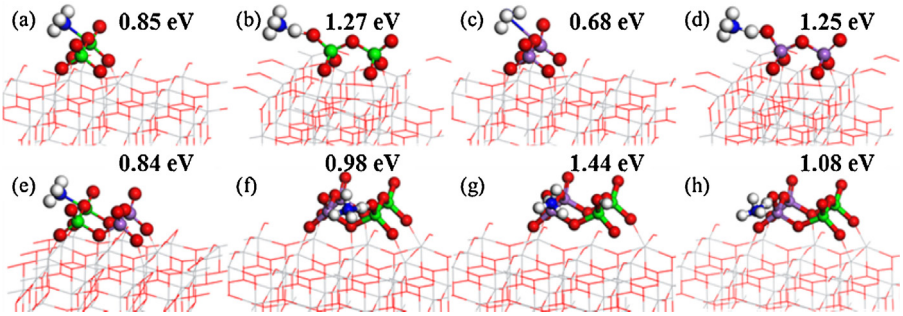

Fig. 5. Structures of NH_3 adsorbed on (a), (b) VTi model, (c), (d) AsTi model, (e)–(h) AsVTi model with Lewis and Brønsted acidity types, respectively. The corresponding adsorption energies are labeled in the figures. Vanadium is green, arsenic is purple, oxygen is red, nitrogen is blue and hydrogen is white. (For interpretation of the references to color in this figure legend, the reader is referred to the web version of this article.)

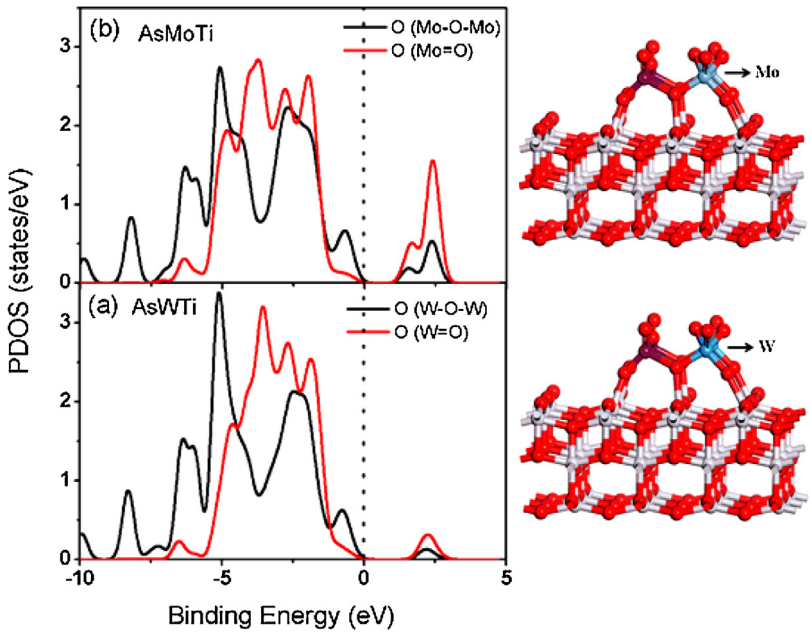

Fig. 6. Projected density of state (PDOS) of O 2p orbitals of M-O-M and M = O for AsMo/Ti and AsW/Ti.

culations. The results suggest that NH_3 molecules are apt to form quite stable adsorptions with arsenic, which agrees with our DRIFTS study (3058 and 3225 cm^{-1}). Combined on both experimental and DFT methods, we propose that total acidity of poisoned catalysts decreases, including quantity of Lewis acid sites and strength of Brønsted acid sites. Though the adsorptions of NH_3 on As–OH are improved and can be served as Brønsted acid sites at 1440 and 3225 cm^{-1}, they are quite stable and less active during SCR process. The PDOS of the NH_3 adsorptions and the distances of N to the clusters are also shown in Figs. S5 and 6.

Fig. 6 shows the PDOS of O 2p states of M–O–M and M = O groups for AsMoTi and AsWTi models, where the MO_3 clusters are neighbored with As_2O_5 cluster on TiO_2 (0 0 1) plane. The conduction band of O 2p for AsWTi is quite smaller than those for AsMoTi, indicating the ability of electron donators is limited when *W* is substituted by Mo. The band gap of AsWTi is slightly larger than that of AsMoTi, implying that the reactivity of both W–O–W and W = O is weak compared with Mo–O–Mo and Mo = O, respectively. This could be one of the factors that MoO_3 has a better arsenic resistance effect than WO_3. Compared with the experimental results, we propose arsenic resistance to the better dispersion of MoO_3 and V_2O_5 on the poisoned catalysts and the maintenance of the reactivity of Mo–O–Mo and Mo = O groups. For V_2O_5–WO_3/TiO_2, amorphous WO_3 aggregate after poisoning, resulting in the decrease of surface acidity and redox property.

4. Conclusion

Based on the experiment and DFT results, two major issues are attempted to propose.

Arsenic at certain loading (1) reduces the surface area and the reducibility of catalysts active sites; (2) the number of Lewis acid sites and the strength of Brønsted acid sites also decrease; (3) new formed As–OH sites only show weak activity above 350 °C. These factors lead to catalysts deactivation.

MoO_3 provides better arsenic poisoning resistance than WO_3 on V_2O_5/TiO_2 catalysts. This could be attributed to the higher dispersion of MoO_3 on the TiO_2 and the synergies effect between Mo and As: the reactivity of Mo–O–Mo and Mo = O groups is considerably higher than that of W–O–W and W = O, respectively. Both the defects of WO_3 lead to significant decrease of surface acidity of V_2O_5–WO_3/TiO_2 after poisoning.

Acknowledgements

The authors gratefully acknowledge the financial supports from National Natural Science Foundation of China (21407088), and National High-Tech Research and the Development (863) Program of China (2013AA065401 and 2013AA065304, the outstanding young scientist funding (21325731) and the international Postdoctoral Exchange Fellowship Program of China (20130032). The authors also appreciate the support from the Brook Byers Institute for Sustainable Systems (BBISS), Hightower Chair and Georgia Research Alliance at Georgia Institute of Technology. The author would also like to thank Prof. Weixue Li and Dr. Chuanqi Huang of Dalian Institute of Chemical Physics in China.

Appendix A. Supplementary data

Supplementary data associated with this article can be found, in the online version, at http://dx.doi.org/10.1016/j.apcatb.2015.08.030.

References

[1] G. Ramis, F. Bregani, Appl. Catal. 64 (1990) 259–278.
[2] N. Topsoe, Science 265 (1994) 1217–1219.
[3] G. Ramis, L. Yi, Catal. Today 28 (1996) 373–380.
[4] G. Busca, L. Lietti, G. Ramis, F. Berti, Appl. Catal. B 18 (1998) 1–36.
[5] L. Lietti, P. Forzatti, G. Ramis, G. Busca, F. Bregani, Appl. Catal. B 3 (1993) 13–35.
[6] W. Kijlstra, M. Biervliet, E. Poels, A. Bliek, Appl. Catal. B 16 (1998) 327–337.
[7] R. Khodayari, C. Odenbrand, Appl. Catal. B 30 (2001) 87–99.
[8] L. Lisi, G. Lasorella, S. Malloggi, G. Russo, Appl. Catal. B 50 (2004) 251–258.
[9] E. Hums, H. Goebel, Ind. Eng. Chem. Res. 30 (1991) 1814–1818.
[10] C. Senior, D. Lignell, A. Sarofim, A. Mehta, Combust. Flame 147 (2006) 209–221.
[11] E. Hums, Catal. Today 42 (1998) 25–35.
[12] Y. Peng, J. Li, X. Huang, X. Li, W. Su, X. Sun, D. Wang, J. Hao, Environ. Sci. Technol. 48 (2014) 4515–4520.
[13] Y. Peng, J. Li, W. Shi, J. Xu, J. Hao, Environ. Sci. Technol. 46 (2012) 12623–12629.
[14] Y. Peng, J. Li, L. Chen, J. Chen, J. Han, H. Zhang, W. Han, Environ. Sci. Technol. 46 (2012) 2864–2869.

[15] Y. Peng, J. Li, W. Si, J. Luo, Y. Wang, J. Fu, X. Li, J. Crittenden, J. Hao, Appl. Catal. B 168–169 (2015) 195–202.
[16] Y. Peng, J. Li, W. Si, J. Luo, Q. Dai, X. Luo, X. Liu, J. Hao, Environ. Sci. Technol. 48 (2014) 13895–13900.
[17] F. Lange, H. Schmelz, H. Knözinger, Appl. Catal. B 8 (1996) 245–265.
[18] E. Hums, Res. Chem. Intermed. 19 (1993) 419–441.
[19] Z. Liu, S. Zhang, J. Li, L. Ma, Appl. Catal. B 144 (2014) 90–95.
[20] Y. Peng, R. Qu, X. Zhang, J. Li, Chem. Commun. 49 (2013) 6215–6217.
[21] V. Avdeev, A. Bedilo, J. Phys. Chem. C 117 (2013) 14701–14709.
[22] M. Calatayud, C. Minot, Top. Catal. 41 (2006) 17–26.
[23] P. Hejduk, M. Szaleniec, M. Witko, J. Mol. Catal. A 325 (2010) 98–104.
[24] X. Du, X. Gao, L. Cui, Z. Zheng, P. Ji, Z. Luo, K. Cen, Appl. Surf. Sci. 270 (2013) 370–376.
[25] X. Du, X. Gao, W. Hu, J. Yu, Z. Luo, K. Cen, J. Phys. Chem. C 118 (2014) 13617–13622.
[26] Z. Wei, S. Zhang, Z. Pan, Y. Liu, Appl. Surf. Sci. 258 (2011) 1192–1198.
[27] K. Alexopoulos, P. Hejduk, M. Witko, M. Reyniers, G. Marin, J. Phys. Chem. C 114 (2010) 3115–3130.
[28] A. Suarez Negreira, J. Wilcox, J. Phys. Chem. C 117 (2012) 1761–1772.
[29] A. Suarez Negreira, J. Wilcox, J. Phys. Chem. C 117 (2013) 24397–24406.
[30] A. Becke, Phys. Rev. A 38 (1988) 3098–3100.
[31] J. Perdew, K. Burke, M. Ernzerhof, Phys. Rev. Lett. 77 (1996) 3865–3868.
[32] B. Delley, Phys. Rev. B 66 (2002) 155125.
[33] J. Graciani, J. Plata, J. Sanz, P. Liu, J. Rodriguez, J. Chem. Phys 132 (2010) 104703.
[34] C. Wang, S. Yang, H. Chang, Y. Peng, J. Li, Chem. Eng. J. 225 (2013) 520–527.
[35] E. Hums, Ind. Eng. Chem. Res. 31 (1992) 1030–1035.
[36] S. Xiong, Y. Liao, X. Xiao, H. Dang, S. Yang, J. Phys. Chem. C 119 (2015) 4180–4187.
[37] X. Wang, A. Shi, Y. Duan, J. Wang, M. Shen, Catal. Sci. Technol. 2 (2012) 1386–1395.
[38] C. Sun, L. Dong, W. Yu, L. Liu, H. Li, F. Gao, L. Dong, Y. Chen, J. Mol. Catal. A 346 (2011) 29–38.
[39] K. Hadjiivanov, Catal. Rev. 42 (2000) 71–144.
[40] L. Wang, W. Li, G. Qi, D. Weng, J. Catal. 289 (2012) 21–29.
[41] Y. Peng, C. Liu, X. Zhang, J. Li, Appl. Catal. B 140–141 (2013) 276–282.
[42] F. Liu, H. He, Catal. Today 153 (2010) 70–76.
[43] F. Liu, H. He, Y. Ding, C. Zhang, Appl. Catal. B 93 (2009) 194–204.
[44] R. Yuan, G. Fu, X. Xu, H. Wan, Phys. Chem. Chem. Phys. 13 (2011) 453–460.